Electron Energy-Loss Spectroscopy (EELS) of Surface Plasmons in Single Silver Nanoparticles and Dimers: Influence of Beam Damage and Mapping of Dark Modes

Ai Leen Koh,[†,*] Kui Bao,[‡] Imran Khan,[†,¶] W. Ewen Smith,[§] Gerald Kothleitner,[⊥] Peter Nordlander,[‡] Stefan A. Maier,[∥] and David W. McComb[†]

[†]Department of Materials, Imperial College London, London SW7 2AZ, United Kingdom, [‡]Laboratory for Nanophotonics and Department of Physics and Astronomy, Rice University, Houston, Texas 77005-1892, [§]Department of Pure and Applied Chemistry, University of Strathclyde, Glasgow G1 1XL, United Kingdom, [⊥]FELMI, Graz University of Technology, Austria, and [∥]Department of Physics, Imperial College London, London SW7 2AZ, United Kingdom. [¶]Current address: AWE, Aldermaston, UK.

ABSTRACT We demonstrate the use of a scanning transmission electron microscope (STEM) equipped with a monochromator and an electron energy loss (EEL) spectrometer as a powerful tool to study localized surface plasmons in metallic nanoparticles. We find that plasmon modes can be influenced by changes in nanostructure geometry and electron beam damage and show that it is possible to delineate the two effects through optimization of specimen preparation techniques and acquisition parameters. The results from the experimental mapping of bright and dark plasmon energies are in excellent agreement with the results from theoretical modeling.

KEYWORDS: electron energy-loss spectroscopy · localized surface plasmon · silver nanoparticles · plasmon hybridization model · scanning transmission electron microscopy

Metallic nanostructures exhibit the phenomenon of localized surface plasmons (LSP) which are oscillations of the conduction electrons coupled to the electromagnetic field.[1] The frequency and intensity of the oscillations are characteristic of the type of material and are highly sensitive to nanostructure geometry and the surrounding medium.[2,3] Applications of nanoplasmonics in areas such as optical data storage[4] and optical wave-guiding[5−7] arise from the ability to control nanoparticle shape and size to produce the desired LSP modes. Changes in geometry can also lead to large enhancements of the incident electromagnetic field at the nanoparticle surface. This effect is being used by the biomedical sciences community to detect single-molecule events[8−10] as well as in surface-enhanced Raman spectroscopy.[11−16]

To realize the potential applications related to plasmonics, it is essential to understand the near-field electromagnetic interactions associated with these nanoparticles, correlate them with geometry, and then tailor their dimensions accordingly. It has been shown that the plasmon resonant energies of complex nanostructures are equivalent to the electromagnetic interactions of plasmons from structures with simpler configurations.[17] Therefore, a thorough understanding of basic systems can facilitate the design of highly sophisticated plasmonic nanostructures with desired optical properties.

A dimer, which consists of two closely spaced nanoparticles, represents the most fundamental system of two interacting objects whose behavior can be explained by the hybridization model.[17,18] When two nanoparticles come into close contact with each other, the plasmon modes of the two nanoparticles interact electromagnetically with each other, resulting in hybridized plasmonic states. The strongest plasmonic couplings occur for longitudinal polarization, where the bonding symmetrically aligned plasmons have finite dipole moments and are commonly referred to as "bright" modes since they can be directly excited by incident light. The higher-energy antibonding modes with their antisymmetric alignment of nanoparticle dipoles possess no net dipole moment and are commonly referred to as "dark" modes. Dark modes include quadrupolar and higher multipolar modes in single nanoparticles,

*Address correspondence to a.koh@imperial.ac.uk.

Received for review August 3, 2009 and accepted September 14, 2009.

Published online September 22, 2009.
10.1021/nn900922z CCC: $40.75

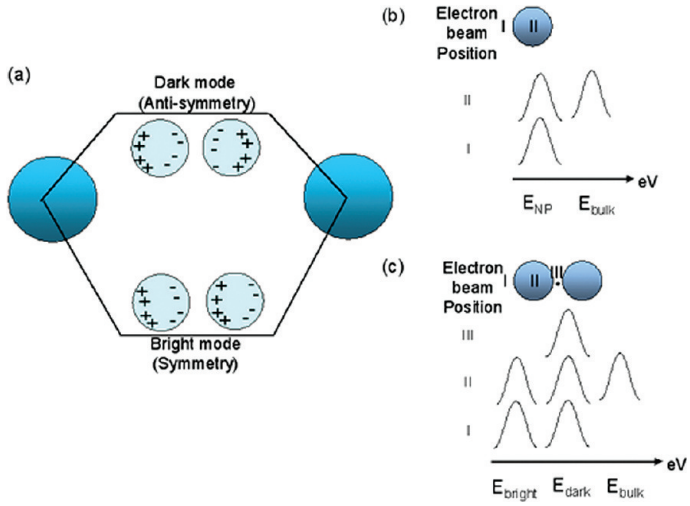

Figure 1. (a) Hybridization model of a symmetric dimer. (b,c) Schematic illustrations of localized plasmon modes as a function of electron probe position for a single nanoparticle and a dimer.

coupled modes with vanishing dipole moments in nanoparticle pairs, and propagating modes in nanoparticle chains and higher-order multipoles. They interact only weakly with the incident light.[19,20] The dark modes are of fundamental interest as they allow for waveguiding on length scales much smaller than the diffraction limit with no radiative losses and can be of importance in biosensing and plasmonic nanolasing applications.[21] Optical studies of dark and higher-order modes have been performed by breaking the symmetry on individual nanoparticles so as to modify the selection rules for plasmon interaction modes.[22,23]

Apart from optical excitation, plasmons can also be generated using electron beams.[24,25] An instrument to study plasmons *via* electron excitation is the scanning transmission electron microscope (STEM). A STEM equipped with an electron energy-loss (EEL) spectrometer and a monochromator represents a powerful method to probe surface plasmons in noble metal nanoparticles because of its high spatial (<1 nm) and energy (<0.2 eV) resolution. The use of a monochromator improves the energy resolution from approximately 0.5 to 0.2 eV and is essential to differentiate the surface and bulk plasmon modes in silver. EEL spectroscopy can reveal plasmon mode patterns with nanometer spatial resolution.[26,27] Moreover, electron impact can excite dark modes in metallic nanostructures.[20] This has been demonstrated by Chu and co-workers[28] who reported the observations of dark modes in gold nanorods. However, data interpretation may be challenging for high-aspect-ratio nanostructures like the above-mentioned because of the splitting of LSP energies into transverse and longitudinal components corresponding to electrons oscillating in directions perpendicular and parallel to the major axis. In the above-mentioned work, the analysis was further compounded by the asymmetric orientation of the nanorod pair.

A simpler and more straightforward system to analyze antisymmetric and other plasmon modes is spherical nanoparticles, which are the focus of this paper. We performed systematic studies to track changes in localized plasmon modes in individual silver nanoparticles and dimers as a function of electron beam position using EELS. All our experimental findings are supported by theoretical modeling, in which a thin dielectric shell was introduced to account for the citrate coating that is commonly found in chemically synthesized silver colloids. We also performed experiments to assess the influence of electron-beam-induced radiation damage on LSP modes, a topic which has received only little attention in the plasmonics community.

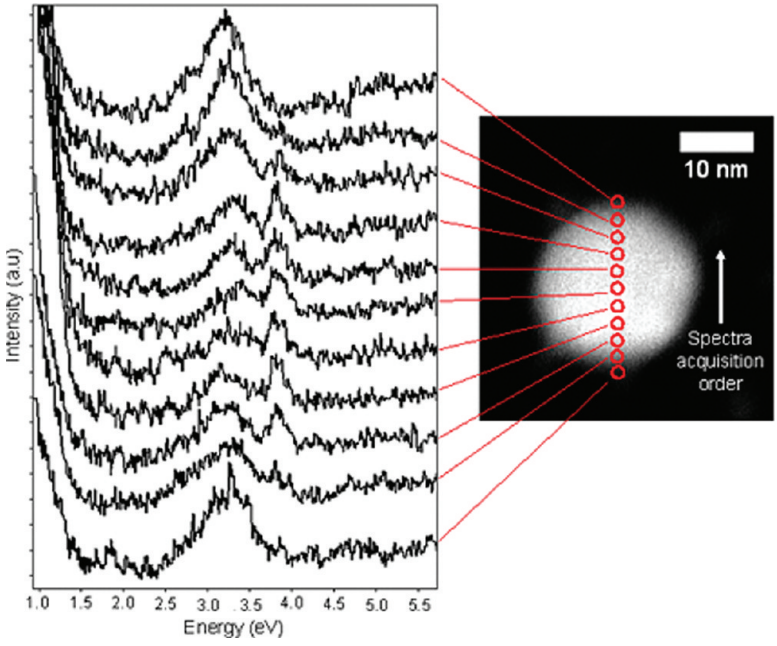

Figure 2. Experimental EELS data of a single silver nanoparticle of diameter approximately 24 nm, showing plasmon energies as a function of electron probe position. The spectra were obtained by positioning the electron probe at 2 nm intervals.

RESULTS AND DISCUSSION

Plasmon Hybridization Model. Figure 1a is a schematic representation of the dimer hybridization model developed by Nordlander and co-workers.[17,18] For polarization along the dimer axis, the interactions between a pair of nanoparticles can be viewed as bonding (bright) and antibonding (dark) combinations of the parent dipolar plasmons. A fast moving charged particle such as an electron in an electron beam induces an electric field in a direction perpendicular to its trajectory. Figure 1b,c shows the plasmon modes that can be excited in an individual nanoparticle and in a dimer as a function of electron beam position. When the electron beam inter-

acts with the particle edge (Position I in Figure 1b), a nanoparticle LSP mode of energy E_{NP} can be excited. When the electron beam passes through the interior of the nanoparticle (Position II in Figure 1b), also the higher-energy bulk plasmon mode E_{bulk} can be excited. The situation holds true for a dimer comprising two particles of equal sizes. However, for a symmetric dimer, the LSP mode can be further decoupled into bright (E_{bright}) and dark (E_{dark}) states. Interaction between the electron and the particle edge (Position I in Figure 1c) can excite both E_{bright} and E_{dark}. For electrons passing through the centers of each particle, all three modes E_{bright}, E_{dark}, and E_{bulk} become excited. For electrons impinging in the center of the dimer junction (Position III in Figure 1c), only the dark (antisymmetric) mode can be excited. The bright mode is symmetry-forbidden because the charges around the electron beam must be of the same sign.

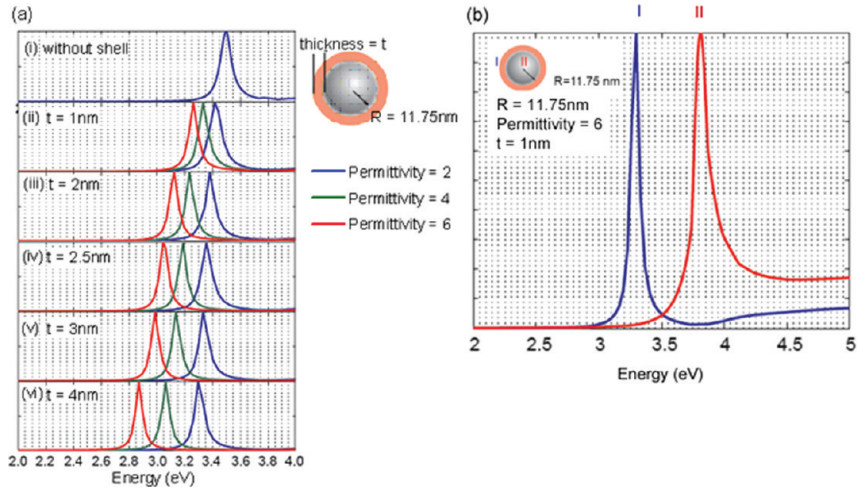

Figure 3. Theoretical model of a single silver nanoparticle. A dielectric shell was included in the model to account for the effects of the citrate coating on the chemically synthesized particle. (a) Changes in localized surface plasmon mode as a function of the thickness of the dielectric shell, *t*, for dielectric permittivity values of 2, 4, and 6. The best fit between experimental and theory is obtained using dielectric permittivity 6 and thickness 1 nm. (b) Polar Mie resonance (I, blue) and bulk plasmon modes (II, red).[29]

Single Nanoparticle. Figure 2 is an experimental EELS data set collected from a single silver nanoparticle with a diameter of approximately 24 nm. Pronounced changes in the spectra as a function of electron beam probe position are revealed. The EEL spectra are collected at 2 nm intervals. The peaks at approximately 3.3 and 3.8 eV correspond to the nanoparticle and bulk plasmon energies of silver which have also been reported by other groups.[29−31] The figure also shows a change in the relative intensities of the surface and bulk plasmon peaks, represented by their relative peak heights, as the beam is shifted from the particle edge to the middle in qualitative agreement with the schematic in Figure 1b.

The measured E_{NP} = 3.3 eV is considerably smaller than the lowest energy dipolar plasmon resonance (3.5 eV) of a silver sphere. The chemically synthesized nanoparticles have a residue of citrate on their surfaces. The properties of a very thin dielectric layer chemisorbed on a surface can be different from a homogeneous system due to charge transfer and chemical interaction effects.[32] Since we do not know the chemical or structural details of this layer, we model the nanoparticle as a homogeneous silver sphere surrounded by a thin uniform dielectric layer. The permittivity and thickness of this layer is then varied until there is good correspondence between the model and experimental data. Figure 3a shows how the LSP energies are shifted when the two parameters were altered. The figure shows that several combinations of shell thickness and dielectric permittivity are possible. The best overall fit between theory and experiment was obtained using a dielectric shell of thickness 1 nm and permittivity of 6. Figure 3b directly compares the dipolar sphere and bulk

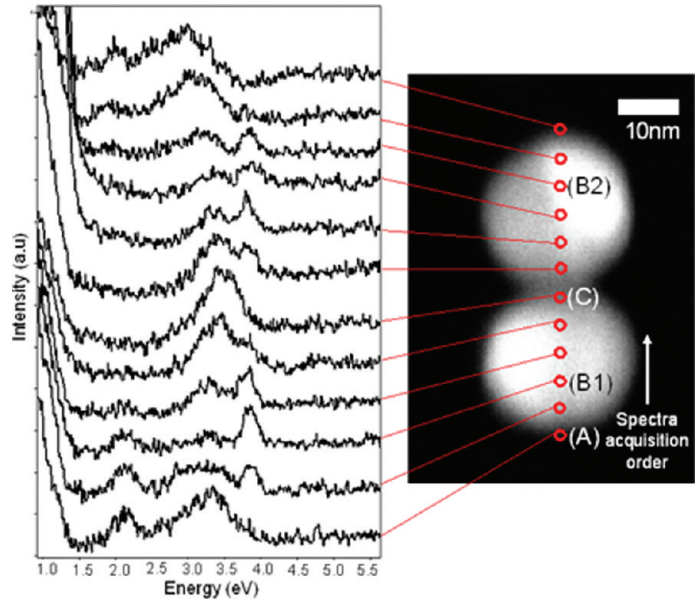

Figure 4. Experimental EELS data set of a symmetrical silver nanoparticle dimer, showing plasmon energies as a function of electron probe position. The spectra are obtained at regular intervals of 4 nm.

plasmon modes for a silver particle surrounded by a 1 nm dielectric of permittivity 6. The inclusion of the carbon film substrate (from the TEM grid) with permittivity 2 and thickness 20 nm and slight deviations in particle shape from the perfect sphere model have negligible effects on the surface plasmon mode (refer to Supporting Information Figure S1).

Symmetric Sphere Dimer. Having established the dielectric permittivity of the citrate shell, we proceeded to investigate the spherical nanoparticle dimer system. Figure 4 shows the EELS data of a silver dimer which is composed of two nanoparticles of approximately the same size. From the high-angle annular dark field

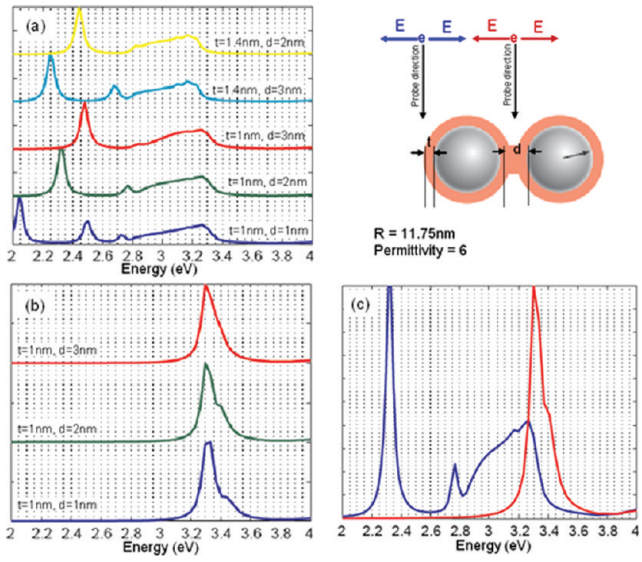

Figure 5. Theoretical model of a silver nanoparticle dimer of radius 11.75 nm and dielectric shell of permittivity 6. (a) Variations in optical spectra as a function of dielectric shell thickness *t* and interparticle distance *d*. The broad peaks around 3.3 eV are due to dipolar and higher-order peaks. The peak shapes are highly sensitive to interparticle distance, as illustrated in (b). (c) Contributions from the electron field at the edge (blue curve) and the intersection (red curve) of a dimer. A dielectric shell of permittivity 6, thickness $t = 1$ nm, and interparticle spacing $d = 2$ nm was used in the computation.

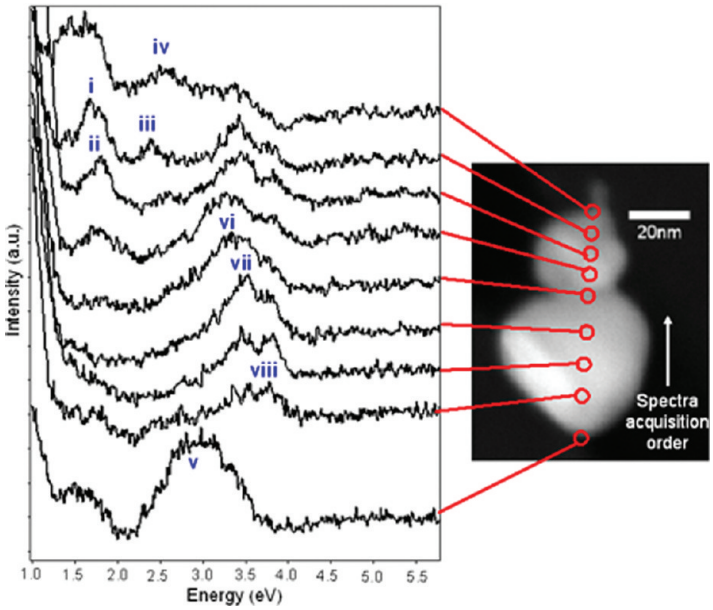

Figure 6. EELS spectra of a heterodimer. The absence of symmetry causes the dimer plasmon energies to exhibit avoided crossings, and both the bonding and antibonding plasmons become dipole-active, leading to multiple peaks in the EEL spectra.

(HAADF)-STEM image on the right, the two particles have radii of approximately 12 nm. The panel on the left shows the EELS spectra obtained at every 4 nm interval. At position A, the beam is nonincident on the particle and two peaks at 2.2 and 3.3 eV, corresponding to the bright and dark modes of the dimer, were observed. The bulk plasmon mode with an energy of 3.8 eV was excited when the probe was incident on the particle, for example, at positions B1 and B2. This energy is the same as our observations from the single nanoparticle and is consistent with the literature.[29−31] At the interface between the particles (*e.g.*, position C), a single peak of 3.4 eV was observed. As the bright mode is symmetry-forbidden, this was interpreted as the dark plasmon mode of the dimer.

The theoretical modeling of the EEL spectra for this dimer is shown in Figure 5. The energy loss spectra are calculated assuming that the electric field from the electrons is perpendicular to the electron trajectory and cylindrically symmetric. The dimer plasmon energies depend sensitively on the interparticle separation (and the dielectric shell thickness *t*). Since it was difficult to define and determine precisely the dimer separation *d* from the STEM image, we treat *d* as a free parameter to be determined by the best fit between calculated and measured LSP energies.

In Figure 5a, we illustrate the strong sensitivity of the EEL spectra on the structural parameters *t* and *d*. An increase in *t* or a reduction in *d* causes all LSP energies to be red-shifted. When the dimer is excited at its interface, the shape of the most intense peak in the antibonding mode becomes sharper with decreasing *d*, as shown in Figure 5b. The calculated EEL spectra for the best fit of $d = 2$ nm is shown in Figure 5c. The contributions of the electron field from the particle edge and at the dimer interface are represented by the blue and red graphs, respectively. The graph in blue shows a dipolar peak at 2.35 eV, a quadrupolar peak at 2.76 eV, and a broad bump consisting of many higher-order peaks around 3.25 eV. In the experimental data (Figure 4), two main peaks at 2.2 and 3.3 eV were observed when the particle edge was excited by the electrons. These are probably the dipolar and higher-order peaks that were predicted from the model. The quadrupolar peak was not visible in the EEL spectra. This could be due to the relatively weak amplitude when it was excited by the electron beam. The red curve in Figure 5b illustrates the effect of the electron field at the intersection between the dimer pair. At this position, the antibonding mode of the dimer is excited. The red curve appears to consist of a single, most intense peak at about 3.3 eV and other peaks of lower intensity. The latter arises from the hybridization of higher-order modes. There is very good correspondence between the most intense peak at 3.3 eV and the single peak of about 3.4 eV that was observed in the EELS spectrum corresponding to position C in Figure 4.

It is also noteworthy to mention that slight deviations of the dimer particles from perfect spheres and the effect of the carbon film substrate (from the TEM grid) have minimal effects on the surface plasmon energies in the symmetric sphere model. For this, we would like to direct the readers to Supporting Information Fig-

ure S2, where one of the particles was modeled as an ellipsoid with a long axis diameter of 24 nm and an orthogonal short axis diameter of 20 nm, and the other as a perfect sphere with a diameter of 24 nm. Slight deviations in particle dimensions and the inclusion of a carbon film substrate of thickness 20 nm and permittivity 2 have minimal effects on the surface plasmon energies.

Asymmetric Nanoparticle Dimer. To further validate the accuracy of the model and its applicability to nonideal systems, we selected a heterodimer system which is composed of two nanoparticles of distinctly different dimensions. Figure 6 shows a HAADF-STEM image of an asymmetric dimer pair which is composed of two particles of diameters 70 and 30 nm. The EELS spectra with corresponding probe positions are illustrated on the left panel. Modes with energies 1.7 eV (i), 1.8 eV (ii), 2.37 eV (iii), 2.5 eV (iv), 3.0 eV (v), 3.3 eV (vi), 3.5 eV (vii), and 3.8 eV (viii) were observed in the data set.

The corresponding theoretical spectra for this heterodimer system are illustrated in Figure 7. By applying the core−shell nanoparticle model, which had been developed and discussed in previous sections, the heterodimer was modeled using two particles with core diameters of 70 and 30 nm and a thin dielectric shell with permittivity value 6. Figure 7a,b illustrates the sensitivity of the EEL spectra to the structural parameters t and d when the particles are excited at the end and center. We obtained an excellent fit between experiment and theory using a shell of thickness $t = 2$ nm and interparticle spacing of $d = 1$ nm.

The calculated EEL spectra for the best fit of $d = 1$ nm are shown in Figure 7c. The contributions of the electron field from the particle edge and at the heterodimer interface are represented by the blue and red graphs, respectively. Peaks i−vii from the experimental data (Figure 6) are indicated in this figure. The bulk plasmon mode of 3.8 eV, which appears as peak viii in Figure 6, does not occur in this model because the bulk mode is not excited when the probe is at a particle edge or heterodimer interface. The numerous plasmon peaks that were observed in both experiment and verified by the theoretical model can be attributed to the breaking of symmetry (parity) when two particles with different dimensions interact with each other.[18]

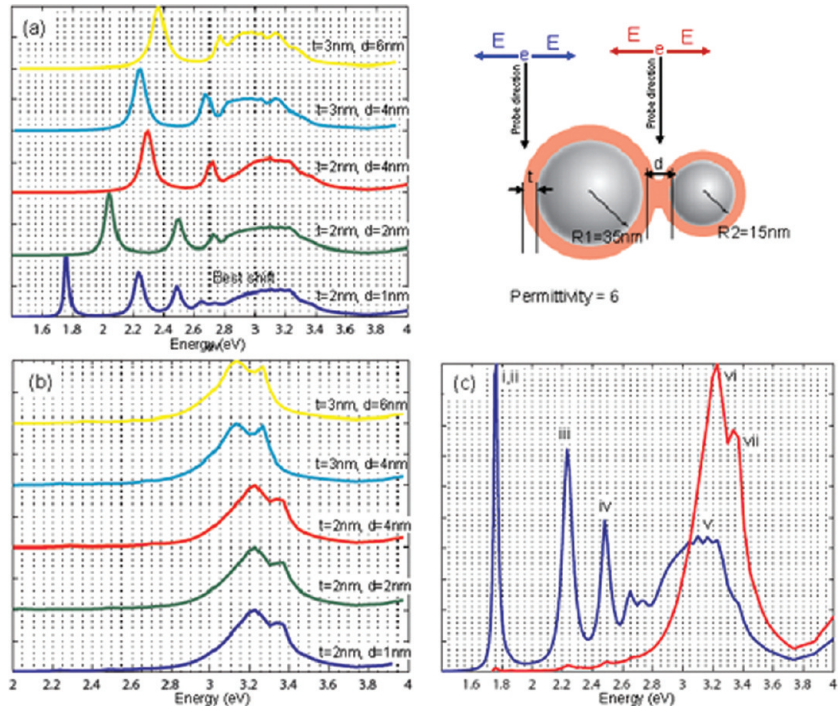

Figure 7. Theoretical model for the heterodimer with core diameters of 70 and 30 nm for electron impact on the side (a) and in the dimer junction (b). The best fit between experiment and theory (c) was obtained using a shell of thickness 2 nm and interparticle spacing of 1 nm in the model.

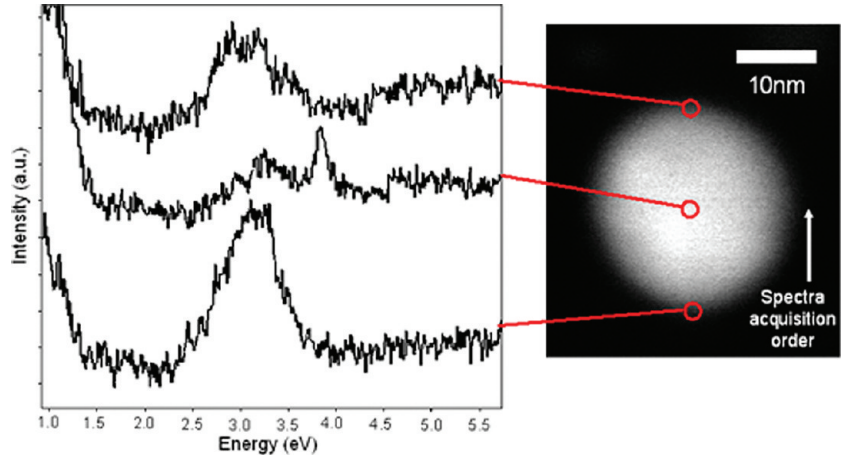

Figure 8. Single silver nanoparticle and its corresponding start, middle, and end EEL spectra. The plasmon peak had red-shifted from 3.2 eV at the beginning of the experiment to 2.95 eV at the end of the acquisition. The nature of the shift is attributed to radiation damage from the electron beam.

The absence of symmetry causes the dimer plasmon energies to exhibit avoided crossings; that is, the dimer plasmon modes repel each other. Both the bonding and antibonding plasmons become dipole-active and are manifested in the form of multiple peaks in the EEL spectra both for end and center excitation.

Influence of Electron Beam Radiation Damage. A concern in analytical electron microscopy is that the interaction between the electron beam and the specimen may cause the latter to be altered, leading to

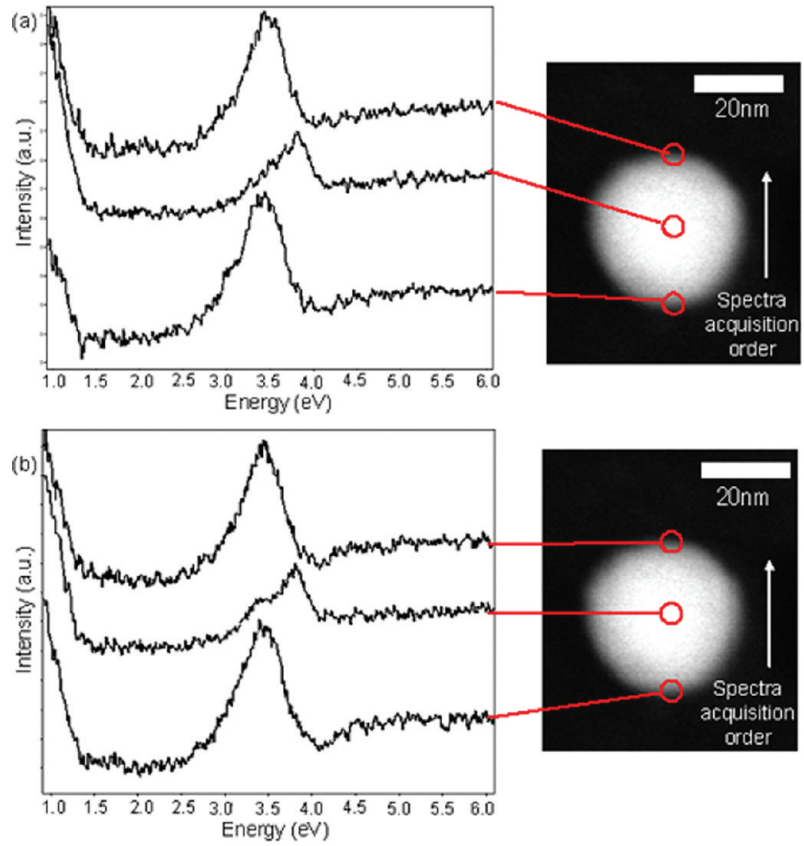

Figure 9. (a) EEL spectra of a particle collected at its start, middle, and end. There is no change between the start and end LSP energies, suggesting that the particle was not damaged by the electron beam. (b) EEL spectra of a particle collected at its start, middle, and end during the second acquisition, where the order (direction) of the second acquisition was the same as the first.

changes in structure, which may in turn affect the shape and peak of the EEL spectra. Generally, electron beam radiation damage can occur in one of two main ways. First, the atoms in the sample may be displaced or even removed, resulting in structural damage and loss of mass. Second, chemical changes in the specimen can result from ionization damage (radiolysis), which subsequently causes a change in structure and a reduction in specimen mass.[33−35]

We are aware that beam damage could become an issue in accurately identifying the LSP modes in nanoparticles. Figure 8 shows three EEL spectra corresponding to the start, middle, and end of a silver nanoparticle that we had studied during the initial stages of our experiment. The plasmon peak had red-shifted from 3.2 eV at the beginning of the experiment to 2.95 eV at the end of the acquisition. Since the particle appeared symmetric morphologically, we attributed the change in LSP energy to damage caused by the electron beam. In particular, because the surface of the particles may consist of residual amounts of organic surfactant (citrate), the rastering of the electron probe across the sample may cause hydrocarbons that were present on both nanoparticle surface and the TEM grid to polymerize, resulting in a thicker layer of carbon buildup at the end of the sample compared to the beginning. The effect is a dampening, or a red shift, in the LSP mode at the end.

We have since been able to optimize specimen preparation techniques, plasma cleaning conditions, and EEL spectra collection times and were able to acquire repeated linescans on the same particles without altering their start and end LSP energies. Figure 9a,b shows the start, middle, and end spectra of a single nanoparticle on which an EEL spectrum was collected at every 2 nm interval. The spectra acquisition was performed twice, and the order (direction) of the second acquisition was the same as the first. There was no noticeable difference in the energy and shape of the EEL spectra in both collections. We also repeated the experiment using a different particle, this time changing the direction of spectra collection for the second time to be opposite to that of the first. The results are shown in Figure 10a,b. There was also no change in the plasmon energies even though signal-to-noise ratios became poorer during the second acquisition (Figure 10b). We therefore conclude that the data presented in our current work delineate all effects of specimen damage from changes in local geometry, and any changes in

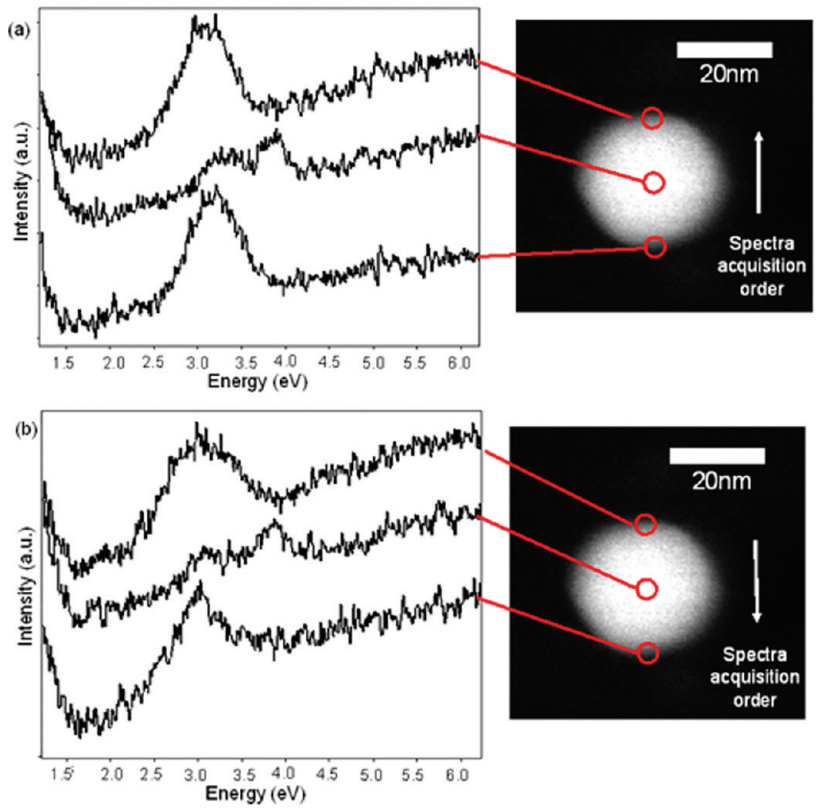

Figure 10. (a) EEL spectra of a particle collected at its start, middle, and end. There is no change between the start and end LSP energies, suggesting that the particle was not damaged by the electron beam. (b) EEL spectra of a particle collected at its start, middle, and end during the second acquisition, where the order (direction) of the second acquisition was opposite compared to the first. There is no change between the LSP energies between the two data sets, but the signal-to-noise ratio during the second acquisition was poorer.

the start and end LSP modes can be attributed to the latter.

CONCLUSIONS

In summary, we have demonstrated the use of monochromated STEM-EELS as a powerful method to study localized plasmon modes in silver nanoparticles. All of our experimental data are in good agreement with theoretical predictions. Plasmon modes are highly sensitive to changes in local geometry and can be influenced by electron beam damage. We have shown that it is possible to minimize the effects of electron beam damage through optimization of specimen preparation techniques and acquisition parameters.

MATERIALS AND METHODS

Silver Nanoparticles. Twenty nanometer (product number R14270-2) and 60 nm (product number R14272-2) colloidal silver nanoparticles were purchased from Agar Scientific Ltd. (Essex, UK). They were manufactured by British Biocell International (Cardiff, UK). The colloids are supplied in water and reported to have trace amounts of sodium citrate dihydrate remaining on the particle surfaces after the synthesis process.

(Scanning) Transmission Electron Microscopy ((S)TEM) and EELS Studies. Specimens were prepared for (S)TEM analyses by first sonicating the silver colloids for 30 min to disperse any contents that may have settled. Five microliters of colloid was pipetted onto 300 mesh copper TEM grids that were coated with a thin network of carbon film (Agar Scientific, product number S166-3). Before the samples were introduced onto the grids, the latter were plasma-cleaned with an Ar/O_2 gas mixture to remove hydrocarbons that might be present. All samples were analyzed using an FEI 80-300 kV Titan operated at 300 kV. It is equipped with a monochromator and a Gatan Tridiem 865 EEL spectrometer with 2048 readout channels. The spatial and energy resolutions of the microscope are 0.3 nm and 0.2 eV, respectively. An aperture size of 100 μm for the third condenser lens system and a camera length of 48 mm were used during EEL spectra acquisition. This is equivalent to a convergence semiangle of 15.1 mrad and a collection semiangle of 17.4 mrad.

EELS spectra were acquired using the line profile feature in the Titan Imaging and Analysis (TIA) software. A high-angle annular dark field (HAADF)-STEM image of the region of interest was first acquired. Then, a line profile was drawn across the nanoparticle(s), and the total number of data points (EELS spectra) was determined such that one spectrum was collected at every 2 nm interval. The cumulative number of spectra per data point is 1. The spectra were acquired with binning 4. Typical collection times for each spectrum ranged from 300 ms for smaller particles to 500 ms for larger particles.

To minimize electron beam damage, oversampling should be avoided. In our experiments, we limited our EEL spectra collection to not more than one spectrum for every 1 nm interval. Other experimental precautions which were taken to minimize electron dose included blanking the electron beam or focusing

the electron probe to a region away from the particles of interest to minimize specimen damage and contamination.

For postprocessing, all data sets were converted into Digital Micrograph-compatible format. The zero loss peak (ZLP) of each spectrum was manually aligned using Digital Micrograph and removed using the reflected tail model. We found that this standard extraction routine within the Digital Micrograph software was not sufficient to completely remove the ZLPs, and the falling tail of the latter still remained in the extracted EEL spectra reported in this paper. Investigations into models to accurately fit and subtract the ZLPs are currently underway.

Theoretical Models and Calculations. Calculations were performed using the commercial FEM software Comsol. The material properties of silver were implemented into the calculations using experimental data from the Johnson and Christy model[36] and by linear interpolation. The excitation source is the field distribution from the electrons. Since the chemically synthesized silver nanoparticles were covered with a layer of citrate coating, they were modeled as core/shell particles. The permittivity value of the dielectric shell used in the models was 6. This was obtained by modeling the nanoparticles with a very thin dielectric shell and then varying its permittivity until there was good agreement between theory and experiment.

Acknowledgment. This work is supported by a Science and Innovation award (EP/D063329) from the Engineering and Physical Sciences Research Council (EPSRC) in the UK, the Robert A. Welch Foundation under Grant C-1222, and the National Science Foundation under Grant CNS-0421109.

Supporting Information Available: Effects of deviation in particle shape and presence of the carbon film substrate (from the TEM grid) on the theoretical optical spectra for a single silver nanoparticle and a silver dimer. This material is available free of charge *via* the Internet at http://pubs.acs.org.

REFERENCES AND NOTES

1. Maier, S. A. *Plasmonics—Fundamentals and Applications*, 1st ed.; Springer: New York, 2007.
2. Kelly, K. L.; Coronado, E.; Zhao, L. L.; Schatz, G. C. The Optical Properties of Metal Nanoparticles: The Influence of Size, Shape, and Dielectric Environment. *J. Phys. Chem. B* **2003**, *107*, 668–677.
3. Mock, J. J.; Barbic, M.; Smith, D. R.; Schultz, D. A.; Schultz, S. Shape Effects in Plasmon Resonance of Individual Colloidal Silver Nanoparticles. *J. Chem. Phys.* **2002**, *116*, 6755–6759.
4. Hashizume, J.; Koyama, F. Plasmon-Enhancement of Optical Near-Field of Metal Nanoaperture Surface-Emitting Laser. *Appl. Phys. Lett.* **2004**, *84*, 3226–3228.
5. Maier, S. A.; Kik, P. G.; Atwater, H. A.; Meltzer, S.; Harel, E.; Koel, B. E.; Requicha, A. A. G. Local Detection of Electromagnetic Energy Transport Below the Diffraction Limit in Metal Nanoparticle Plasmon Waveguides. *Nat. Mater.* **2003**, *2*, 229–232.
6. Dawson, P.; Puygranier, B. A. F.; Goudonnet, J.-P. Surface Plasmon Polariton Propagation Length: A Direct Comparison Using Photon Scanning Tunneling Microscopy and Attenuated Total Reflection. *Phys. Rev. B* **2001**, *63*, 205410.
7. Maier, S. A. Plasmonics: The Promise of Highly Integrated Optical Devices. *IEEE J. Sel. Top. Quantum Electron.* **2006**, *12*, 1671–1677.
8. Nie, S. M.; Emory, S. R. Probing Single Molecules and Single Nanoparticles by Surface-Enhanced Raman Scattering. *Science* **1997**, *275*, 1102–1106.
9. Kneipp, K.; Wang, Y.; Kneipp, H.; Perelman, L. T.; Itzkan, I.; Dasari, R. R.; Feld, M. S. Single Molecule Detection Using Surface-Enhanced Raman Scattering (SERS). *Phys. Rev. Lett.* **1997**, *78*, 1667–1670.
10. Sannomiya, T.; Hafner, C.; Voro., J. *In Situ* Sensing of Single Binding Events by Localized Surface Plasmon Resonance. *Nano Lett.* **2008**, *8*, 3450–3455.
11. Lal, S.; Link, S.; Halas, N. J. Nano-optics From Sensing to Waveguiding. *Nat. Photonics* **2007**, *1*, 641–648.
12. Moskovits, M.; Jeong, D. H. Engineering Nanostructures for Giant Optical Fields. *Chem. Phys. Lett.* **2004**, *397*, 91–95.
13. Kneipp, K.; Kneipp, H.; Itzkan, I.; Dasari, R. R.; Feld, M. S. Surface Enhanced Raman Scattering and Biophysics. *J. Phys.: Condens. Mater.* **2002**, *14*, R597–R624.
14. Xu, H.; Käll, M. Polarization-Dependent Surface-Enhanced Raman Spectroscopy of Isolated Silver Nanoaggregates. *Chem. Phys. Chem.* **2003**, *4*, 1001–1005.
15. Xu, H.; Bjerneld, E. J.; Käll, M.; Borjesson, L. Spectroscopy of Single Hemoglobin Molecules by Surface Enhanced Raman Scattering. *Phys. Rev. Lett.* **1999**, *83*, 4357–4360.
16. Xu, H.; Aizpurua, J.; Käll, M.; Apell, P. Electromagnetic Contributions to Single-Molecule Sensitivity in Surface-Enhanced Raman Scattering. *Phys. Rev. E* **2000**, *62*, 4318–4324.
17. Prodan, E.; Nordlander, P. Plasmon Hybridization in Spherical Nanoparticles. *J. Chem. Phys.* **2004**, *120*, 5444–5454.
18. Nordlander, P.; Oubre, C.; Prodan, E.; Li, K.; Stockman, M. I. Plasmon Hybridization in Nanoparticle Dimers. *Nano Lett.* **2004**, *4*, 899–903.
19. Marton, J. P.; Jordan, B. D. Optical Properties of Aggregated Metal Systems: Interband Transitions. *Phys. Rev. B* **1977**, *15*, 1719–1727.
20. Liu, M.; Lee, T.-W.; Gray, S. K.; Guyot-Sionnest, P.; Pelton, M. Excitation of Dark Plasmons in Metal Nanoparticles by a Localized Emitter. *Phys. Rev. Lett.* **2009**, *102*, 107401.
21. Zheludev, N. I.; Prosvirnin, S. L.; Papasimakis, N.; Fedotov, V. A. Lasing Spaser. *Nat. Photonics* **2008**, *2*, 351–354.
22. Wang, H.; Wu, Y.; Lassiter, B.; Nehl, C. L.; Hafner, J. H.; Nordlander, P.; Halas, N. J. Symmetry Breaking in Individual Plasmonic Nanoparticles. *Proc. Natl. Acad. Sci. U.S.A.* **2006**, *103*, 10856–10860.
23. Verellen, N.; Sonnefraud, Y.; Sobhani, H.; Hao, F.; Moshchalkov, V. V.; Van Dorpe, P.; Nordlander, P.; Maier, S. A. Fano Resonances in Individual Coherent Plasmonic Nanocavities. *Nano Lett.* **2009**, *9*, 1663–1667.
24. Ritchie, R. H. Plasma Losses by Fast Electrons in Thin Films. *Phys. Rev.* **1957**, *106*, 874–881.
25. Stern, E. A.; Ferrell, R. A. Surface Plasma Oscillations of a Degenerate Electron Gas. *Phys. Rev.* **1960**, *120*, 130–136.
26. Nelayah, J.; Kociak, M.; Stephan, O.; Garcia de Abajo, F. J.; Tence, M.; Henrard, L.; Taverna, D.; Pastoriza-Santos, I.; Liz-Marzan, L. M. Colliex. Mapping Surface Plasmons on a Single Metallic Nanoparticle. *Nat. Phys.* **2007**, *3*, 348–353.
27. Bosman, M.; Keast, V. J.; Watanabe, M.; Maaroof, A. I.; Cortie, M. B. Mapping Surface Plasmons at the Nanometre Scale with an Electron Beam. *Nanotechnology* **2007**, *18*, 165505.
28. Chu, M.-W.; Myroshnychenko, V.; Chen, C. H.; Deng, J.-P.; Mou, C.-Y.; Garcia de Abajo, F. J. Probing Bright and Dark Surface-Plasmon Modes in Individual and Coupled Noble Metal Nanoparticles Using an Electron Beam. *Nano Lett.* **2009**, *9*, 399–404.
29. Pulisciano, A.; Park, S. J.; Palmer, R. E. Surface Plasmon Excitation of Au and Ag in Scanning Probe Energy Loss Spectroscopy. *Appl. Phys. Lett.* **2008**, *93*, 213109.
30. Barman, S. R.; Biswas, C.; Horn, K. Electronic Excitations on Silver Surfaces. *Phys. Rev. B* **2004**, *69*, 045413.
31. Ouyang, F.; Batson, P. E.; Isaacson, M. Quantum Size Effects in the Surface-Plasmon Excitation of Small Metallic Particles by Electron-Energy-Loss Spectroscopy. *Phys. Rev. B* **1992**, *46*, 15421–15425.
32. Mulvaney, P. Surface Plasmon Spectroscopy of Nanosized Metal Particles. *Langmuir* **1996**, *12*, 788–800.
33. Kirkland, A.; Hutchison, J. *Nanocharacterization*; Royal Society of Chemistry: UK, 2007.
34. Egerton, R. F.; Li, P.; Malac, M. Radiation Damage in the TEM and SEM. *Micron* **2004**, *35*, 399–409.
35. Egerton, R. F.; Wang, F.; Crozier, P. A. Beam-Induced Damage to Thin Specimens in an Intense Electron Probe. *Microsc. Microanal.* **2006**, *12*, 65–71.
36. Johnson, P. B.; Christy, R. W. Optical Constants of the Noble Metals. *Phys. Rev. B* **1972**, *6*, 4370–4379.